

# Bu-Shen-Ning-Xin decoction inhibits macrophage activation to ameliorate premature ovarian insufficiency-related osteoimmune disorder *via* FSH/FSHR pathway

Hongmei Sun<sup>1,2,3,4,§</sup>, Qing Qi<sup>5,§</sup>, Xinyao Pan<sup>1,2,3</sup>, Jing Zhou<sup>1,2,3</sup>, Jing Wang<sup>1,2,3</sup>, Lisha Li<sup>1,2,3</sup>, Dajing Li<sup>1,2,3</sup>, Ling Wang<sup>1,2,3,\*</sup>

<sup>1</sup>Laboratory for Reproductive Immunology, Obstetrics and Gynecology Hospital of Fudan University, Shanghai, China;

<sup>2</sup>The Academy of Integrative Medicine of Fudan University, Shanghai, China;

<sup>3</sup>Shanghai Key Laboratory of Female Reproductive Endocrine-related Diseases, Shanghai, China;

<sup>4</sup>Hexi University, Zhangye, Gansu, China;

<sup>5</sup>Wuhan Business University, Wuhan, Hubei, China.

**SUMMARY** Limited studies are associated with premature ovarian insufficiency (POI)-related osteoimmune disorder currently. Bu-Shen-Ning-Xin decoction (BSNXD) displayed a favorable role in treating postmenopausal osteoporosis. However, its impact on the POI-related osteoimmune disorder remains unclear. The study primarily utilized animal experiments and network pharmacology to investigate the effects and underlying mechanisms of BSNXD on the POI-related osteoimmune disorder. First, a 4-vinylcyclohexene dioxide (VCD)-induced POI murine model was conducted to explore the therapeutical action of BSNXD. Second, we analyzed the active compounds of BSNXD and predicted their potential mechanisms for POI-related osteoimmune disorder *via* network pharmacology, further confirmed by molecular biology experiments. The results demonstrated that VCD exposure led to elevated follicle-stimulating hormone (FSH) levels, a 50% reduction in the primordial follicles, bone microstructure changes, and macrophage activation, indicating an osteoimmune disorder. BSNXD inhibited macrophage activation and osteoclast differentiation but did not affect serum FSH and estradiol levels in the VCD-induced POI model. Network pharmacology predicted the potential mechanisms of BSNXD against the POI-related osteoimmune disorder involving tumor necrosis factor  $\alpha$  and MAPK signaling pathways, highlighting BSNXD regulated inflammation, hormone, and osteoclast differentiation. Further experiments identified BSNXD treatment suppressed macrophage activation *via* downregulating FSH receptor (FSHR) expression and inhibiting the phosphorylation of ERK and CCAAT enhancer binding proteins  $\beta$ . In conclusion, BSNXD regulated POI-related osteoimmune disorder by suppressing the FSH/FSHR pathway to reduce macrophage activation and further inhibiting osteoclastogenesis.

**Keywords** premature ovarian insufficiency, Bu-Shen-Ning-Xin decoction, osteoimmune disorder; network pharmacology, macrophages, osteoclastogenesis

## 1. Introduction

Premature ovarian insufficiency (POI), commonly called premature ovarian failure before, is a disease characterized by menopause or sparse menstruation, elevated follicle-stimulating hormone (FSH), and loss of oocytes and folliculogenesis, affecting 3.7% or more of women under age 40 (1,2). POI involves a higher risk of infertility, osteoporosis, cardiovascular disease, and a decline in cognitive function (3-5); however, studies usually focus on the poor reproductive potential

in POI (3,4), and little is associated with POI-related osteoporosis currently. Therefore, studies are needed to explore the pathogenesis of POI-related osteoporosis, and strategies are imperative for the disease.

Elevated FSH levels, pointing to the decline of ovarian function, affected the bone immune microenvironment. FSH and bone mineral density (BMD) have a negative correlation (6). Likewise, the biochemical markers of bone turnover, including osteocalcin and serum bone-specific alkaline phosphatase, were positively correlated with sharply elevated FSH (7), which can enhance bone

resorption independent of estrogen (8,9). Mechanically, FSH stimulates tumor necrosis factor (TNF) production from the monocytes to enhance osteoclast formation, involving the MEK/ERK and CCAAT enhancer binding proteins (C/EBP)  $\beta$  signaling pathways (10,11).

Traditional Chinese medicine (TCM) has rich experience and unique advantages in treating POI due to its multi-component and multi-target action. Several studies highlighted the clinical efficacy of TCM compounds on POI or osteoporosis (12,13). Bu-Shen-Ning-Xin decoction (BSNXD), formulated on clinical experience over the decades and comprising eight herbal medicines, has been used for treating postmenopausal osteoporosis (14). In our previous works, BSNXD ameliorated postmenopausal osteoporosis by blocking the nuclear factor of activated T-cells 1 (NFATc1) pathway to inhibit osteoclast differentiation (15,16). Moreover, BSNXD could modulate receptor activator of nuclear factor- $\kappa$ B ligand (RANKL)/osteoprotegerin imbalance by regulating the immunocyte function (17). Nonetheless, the effects and mechanisms of BSNXD in regulating POI-related osteoimmune disorder are unclear.

This work explored the effects of BSNXD in a 4-vinylcyclohexene dioxide (VCD)-induced murine model, which successfully simulates a POI-related osteoimmune disorder (18,19). Then, we analyzed the active compounds of BSNXD and predicted its potential mechanisms on the POI-related osteoimmune disorder *via* network pharmacology, which explores the herbs' pharmacological mechanisms based on system biology and bioinformatics (20). Finally, we utilized molecular biology experiments to validate the molecular mechanism.

## 2. Materials and Methods

### 2.1. Animal experiments

#### 2.1.1. Reagents

4% paraformaldehyde was purchased from Shanghai USEN Biological Technology Co., Ltd. (Shanghai, China). Estradiol (E2) parameter assay kit was obtained from R&D System, Inc. (Minneapolis, MN, USA). An enzyme-linked immunosorbent assay kit for FSH was obtained from Cloud-Clone Corp. (Wuhan, China). Tissue RNA extraction kits, reverse transcription-PCR kit, and SYBR Green quantitative PCR assay mix were purchased from HiFun Biotechnology Co., Ltd. (Shanghai, China). Anti-CD16/CD32, PE anti-mouse MHCII, PE anti-mouse CD86, FITC anti-mouse/human CD11b, and APC anti-mouse F4/80 antibodies were provided by Biologend, Inc. (CA, USA). APC-Cy7 anti-mouse CD45 and BV605 anti-mouse CD3e antibodies were obtained from BD Biosciences (NJ, USA). LIVE/DEAD™ fixable dead cell stain kit and FSH receptor (FSHR) polyclonal antibody were obtained from Thermo

Fisher Scientific, Inc. (MA, USA). RIPA and protease inhibitors were obtained from New Cell & Molecular Biotech Co., Ltd. (Suzhou, China). pC/EBP $\beta$  and pERK1-T202/Y204 rabbit antibodies were purchased from ABclonal Technology Co., Ltd. (Wuhan, China). Toluidine blue staining solution and tartrate-resistant acid phosphatase (TRAP) dye solution kit were acquired from Servicebio Technology Co., Ltd. (Wuhan, China). Rabbit antibody against tubulin and goat anti-rabbit secondary antibodies were purchased from Proteintech Group, Inc. (Rosemount, IL, USA).

#### 2.1.2. Preparation of BSNXD extracts

Chinese medicine formula granules in BSNXD were obtained from Tianjiang Pharmaceutical Co., Ltd. (Jiangsu, China). The composition and dosage of BSNXD are listed in Table 1. All voucher specimens were deposited and quantified for quality control at the Obstetrics and Gynecology Hospital of Fudan University. Our previous study analyzed the UPLC fingerprint and the multi-component content of BSNXD (14).

#### 2.1.3. Animals and treatment

Thirty female C57BL/6 mice aged 6-8 weeks (Vital River Laboratory Animal Technology Co., Ltd., Zhejiang, China) were adaptively fed in carbonate plastic cages in the Fudan University laboratory (SPF grade) animal room for one week. The environment was kept temperature- and humidity-controlled. The mice were fed a commercial product (Jiangsu Synergetic Pharmaceutical Bioengineering Co., Ltd.). All procedures are carried out in accordance with the requirements of the Laboratory Animal Care Principles (National Institutes of Health Publication No. 85-23, revised 1985) and guidelines for care and use of Fudan University Laboratory Animal (approval number: 2022120016S).

The mice were randomly divided into the control, model, and BSNXD groups ( $n = 10$  in each group). VCD (160 mg/kg/day) was injected intraperitoneally for 15 consecutive days to establish the POI model (18). The model and BSNXD groups were given VCD while the control group was given saline for 15 days. At the same

**Table 1. Composition and dosage of BSNXD**

Chinese name	Latin name	Content (g)
Di-Huang	<i>Rehmannia glutinosa</i> (Gaertn.) DC.	15
Zhi-Mu	<i>Anemarrhena asphodeloides</i> Bunge	15
Huang-Bai	<i>Phellodendron chinense</i> C.K.Schneid.	9
Gou-Qi	<i>Lycium chinense</i> Mill.	15
Tu-Si-Zi	<i>Cuscuta chinensis</i> Lam.	12
Yin-Yang-Huo	<i>Epimedium brevicornu</i> Maxim.	12
Suan-Zao	<i>Ziziphus jujuba</i> var. <i>spinosa</i> (Bunge) Hu ex H.F.Chow.	9
Ze-Xie	<i>Alisma plantago-aquatica</i> L.	12

time, the mice in the BSNXD group were intragastrically administered with BSNXD (1.287 g/kg) daily, and the mice in the control and model groups were given sterile water. Animals were sacrificed under fluoroethane anesthesia on the 30th after the last injection of VCD. Then, ovaries, blood, femurs, tibia, vertebrae, spleen, and mesenteric lymph nodes were collected for further study. The murine body weights were recorded weekly.

#### 2.1.4. Serum FSH and E2 levels measurement

Blood was collected through cardiac puncture, solidified in 2 hours at room temperature, and then centrifuged to obtain serum. In accordance with protocols from the manufacturers, serum E2 and FSH levels were detected with an E2 parameter assay kit and an enzyme-linked immunosorbent assay kit for FSH, respectively.

#### 2.1.5. Hematoxylin and eosin (H&E) staining

The murine ovarian was exfoliated, fixed in 4% paraformaldehyde, dehydrated, and embedded in paraffin. Five  $\mu\text{m}$  paraffin-embedded samples were then sectioned for further H&E staining. H&E-stained segments were observed under an optical microscope (Nikon, Japan) to analyze the morphological changes and follicle count according to the classification standard (21).

#### 2.1.6. Micro-computed tomography (micro-CT) scanning and analysis

Murine femurs and vertebrae were fixed with 4% paraformaldehyde. Then, the tissues were scanned and analyzed by micro-CT (SKYSCAN 1176 scanner, Bruker Corporation) at 50 kV voltage and 500  $\mu\text{A}$  current with a scanning parameter of 9  $\mu\text{m}$  per layer. The mouse femur and fourth lumbar vertebra were used for analysis. The bone microstructure parameters were obtained according to the relevant three-dimensional

(3D) images in the CTAn software (Bruker micro-CT, Kontich, Belgium) (22).

#### 2.1.7. Immunohistochemistry

The fixed murine tibias were proceeded for decalcification with ethylenediaminetetraacetic acid for the TRAP staining, following the steps required by the manufacturer. The undecalcified murine tibias were used for the toluidine blue staining following the instructions. Two pathologists independently and double-blindly observed histological changes using a microscope (OLYMPUS, Tokyo, Japan).

#### 2.1.8. Quantitative reverse transcription polymerase chain reaction

Total RNA was extracted from the homogenized bone tissue using a tissue RNA purification kit. The cDNA was synthesized using a reverse transcription kit. We performed quantitative real-time PCR in triplicate with an SYBR premix ex taq kit on an Applied Biosystems 7900 HT system (Foster City, CA, USA). The relative mRNA expression was calculated using the  $2^{-\Delta\Delta C_t}$  method. Mouse primers listed in Table 2 were synthesized by Huagene Biotech (Shanghai, China).

#### 2.1.9. Flow cytometry

Single-cell suspensions from spleen, mesenteric lymph nodes, or bone marrow were stained with a LIVE/DEAD™ fixable yellow dead cell stain kit and blocked with anti-CD16/CD32 antibody. Then, the cells were washed in phosphate-buffered saline solution and incubated with antibody cocktails. The antibody cocktails included PE anti-mouse MHCII, FITC anti-mouse/human CD11b, PE anti-mouse CD86, APC anti-mouse F4/80, APC-Cy7 anti-mouse CD45, or BV605 anti-mouse CD3e. The stained cells were analyzed on a

**Table 2. Primers used in this study**

Gene	Forward primer	Reverse primer
<i>Fshr</i>	CCTTGCTCCTGGTCTCCTTG	CTCGGTCACCTTGCTATCTTG
<i>Trap</i>	CAAGAACTTGGCACCATTGTTA	ATCCATAGTGAAACCGCAAGTA
<i>Ctsk</i>	CTGAGAATGTGGCTGTGGAG	TACCCTCTGCATTTAGCTGCCT
<i>Mmp9</i>	GCAGAGGCATACTTGTACCG	TGATGTTATGATGGTCCCACCTTG
<i>c-fos</i>	TCTCTAGTGCCAACTTTATCCC	GAGATAGCTGCTCTACTTTGCC
<i>Nfatc1</i>	GAGAATCGAGATCACCTCCTAC	TTGCAGCTAGGAAGTACGTCTT
<i>C/ebp<math>\beta</math></i>	CCAAGCCGAGCAAGAAGC	AGGGCGAACGGGAAACCG
<i>Rankl</i>	CAAGATGGCTTCTATTACCTGT	TTGATGCTGGTTTTAACGAC
<i>Tnfa</i>	TATGGCCAGACCCCTACA	GGAGTAGACAAGGTACAACCCATC
<i>Il6</i>	CTTCTTGGGACTGATGCTGGTGAC	TCTGTTGGGAGTGGTATCCTCTGTG
<i>Il1<math>\beta</math></i>	AAAAAGCCCTCGTGTGTCGG	GTGGGTGTGCCGTCTTTCAT
<i>Ccl2</i>	TTAAAAACCTGGATCGGAACCAA	GCATTAGCTTCAGATTACGGGT
<i><math>\beta</math>-actin</i>	GGCTGTATTCCCCTCCATCG	CCAGTTGGTAACAATGCCATGT

Ccl: chemokine (CC-motif) ligand; Cebp: CCAAT enhancer binding protein; Ctsk: cathepsin K; Fshr: follicle-stimulating hormone receptor; IL: interleukin; Mmp9: matrix metalloprotein 9; Nfatc1: nuclear factor of activated T-cells 1; Rankl: receptor activator of nuclear factor- $\kappa$ B ligand; Tnf: tumor necrosis factor; Trap: tartrate-resistant acid phosphatase.

CytoFLEX (Beckman Coulter, Inc., CA, USA). FlowJo software (Tree Star, Ashland, OR, USA) was utilized to analyze data.

#### 2.1.10. Western blotting

The supernatant was collected from the lysed bone tissue and quantified using a BCA protein detection kit. The protein samples were separated by electrophoresis and transferred to a polyvinylidene fluoride membrane. The membrane was incubated with anti-FSHR, anti-pC/EBP $\beta$ , anti-pERK, or anti-tubulin primary antibodies at 4°C overnight after being blocked by 5% skim milk powder solution. The next day, the membrane was washed with TBST solution and incubated with a secondary antibody at room temperature. Protein-binding bands are displayed using an ECL reagent on an Amersham Imager 600 (GE Healthcare Life Sciences, MA, USA). Image J (NIH, USA) was performed for quantitative analysis.

### 2.2. Pharmacological network analysis

#### 2.2.1. Screening the active chemical compound and potential targets of BSNXD

We screened the potential active ingredients of BSNXD under the following filter criteria: Oral bioavailability  $\geq$  30% and Drug likeness  $\geq$  0.18 in the HERB (<http://herb.ac.cn>) and TCM systematic pharmacology database and analysis platform (TCMSP, <https://www.tcmsp-e.com/tcmsp.php>). The bioactive compound-related targets were collected from TCMSP and standardized through the UniProt database (<https://www.uniprot.org>). Then, we imported active components and associated gene data into Cytoscape 3.7.2 to build a component-target gene network.

#### 2.2.2. Collection of potential targets of POI-related osteoimmune disorder

The POI and osteoimmune disorder-related targets were obtained from the Disgenet (<https://www.disgenet.org/home/>), OMIM (<https://www.omim.org/>), and GeneCards (<https://www.genecards.org>) databases with the keyword "premature ovarian insufficiency" and "osteoimmune disorder." The overlapped genes were chosen as the targets of BSNXD against POI-related osteoimmune disorder using Venny 2.1.0 (<http://www.liuxiaoyuuan.cn/>).

#### 2.2.3. Network construction

The overlapped targets were inputted into the STRING database (<https://cn.string-db.org/>). The species was set as "homo sapiens," and the confidence score was set to  $> 0.4$ . A protein-protein interaction (PPI) network of the overlapped targets was re-edited and visualized in the

Cytoscape 3.7.2 software. Topology attribute parameters are calculated using Cytohubba and cytoNCA plugins, which were used to obtain the top 20 targets and rebuild the critical network.

#### 2.2.4. Enrichment analysis

The overlapped targets were fed into the Metascape database (<https://metascape.org/>) for the Gene Ontology (GO) and Kyoto Encyclopedia of Genes and Genomes (KEGG) enrichment analysis. The involved biological processes and signaling pathways were visualized by bubble charts and bar charts with  $P$ -value  $< 0.05$ , enrichment factor  $> 1.5$ , and minimum count of 3.

### 2.3. Statistical analysis

Data are displayed as mean  $\pm$  SD. Comparisons were evaluated by  $t$ -test or one-way ANOVA followed by Dunnett's multiple comparisons tests using GraphPad Prism version 8.0 for Windows (GraphPad Software, Inc., San Diego, CA, USA). A  $P$ -value less than 0.05 was statistically significant.

## 3. Results

### 3.1. BSNXD slightly ameliorated the ovarian dysfunction in the VCD-induced POI model

To explore the effects of BSNXD, we established a VCD-induced POI murine model. VCD and BSNXD had little impact on body weight (Figure 1A). Since the disorder of sex hormones plays a crucial role in POI progression, the levels of serum FSH and E2 were measured to investigate the murine ovarian function. As shown in Figures 1B-1C, serum FSH and E2 levels increased sharply when mice were exposed to VCD. BSNXD slightly downregulated the serum level of FSH; however, the levels of serum FSH and E2 remained indistinguishable between the model and BSNXD groups (Figures 1B-1C). VCD selectively destroys the primordial and primary follicles, gradually depleting the murine follicle pool (18). At 30 days after the last VCD injection, we measured the wet weight of the ovaries and calculated the ovarian index. VCD exposure decreased the murine ovarian index (Figure 1D) and led to a 50% reduction in the primordial follicles and a decrease in other types of follicles (Figure 1E), indicating VCD successfully induced ovarian failure. BSNXD treatment markedly improved the ovarian index (Figure 1D) and saved part of the primordial and primary follicles (Figures 1E-1F).

### 3.2. BSNXD improved the bone microstructure parameters in the murine vertebrae

Long-term elevated FSH levels contribute to

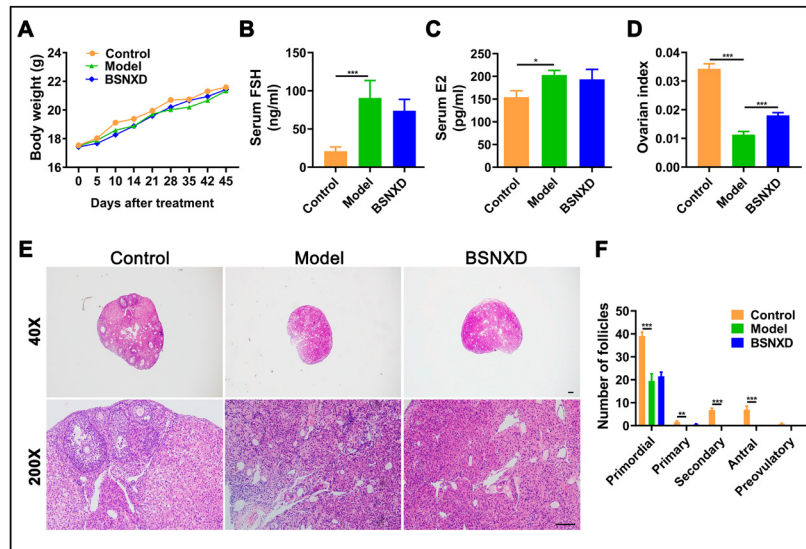


**Figure 1.** The effects of BSNXD on body weight, serum hormones, and ovaries. (A) Body weight. (B–C) The serum levels of FSH (B) and E2 (C). (D) Ovarian index. (E) Representative images of H&E-stained ovarian sections at different magnifications. Scale bars are 100  $\mu$ m. (F) The follicle numbers were quantified in ovaries.  $n = 5$ . \* $P < 0.05$ , \*\* $P < 0.01$ , \*\*\* $P < 0.001$ .

osteoporosis risk in women with menopause transition (9). To investigate whether VCD exposure induced bone morphological changes and reduced bone density, one of the common POI complications, we utilized micro-CT scanning to reconstruct clear 3D images of the murine vertebrae and femur. As shown in Figure 2A, the trabecular bone structure of the control mice was clear, rich, and continuous, connecting into a network; however, an enlarged trabecular separation (Tb.Sp) and trabecular bone volume fraction were observed in the model mice. Notably, BSNXD treatment decreased the bone parameters, including bone surface/bone volume (BS/BV, Figure 2B), Tb.Sp (Figure 2F), structure model index (SMI, Figure 2G), and trabecular bone pattern factor (Tb.Pf, Figure 2H). Meanwhile, BSNXD treatment markedly elevated trabecular thickness (Tb.Th, Figure 2E) and mildly raised the values of bone volume/tissue volume (BV/TV, Figure 2C) and trabecular number (Tb.N, Figure 2D). Next, we measured the murine spine BMD to evaluate bone loss. There was a mild reduction of spine BMD in the VCD-induced mice, but BSNXD treatment slightly improved the spine BMD (Figure 2I).

### 3.3. BSNXD improved the bone microstructure parameters in the murine femur

We also further analyzed the bone microstructure of the murine femur (Figures 3A–3B). Apparent voids among bone trabeculae in the cancellous bone were observed in the murine femur in the model group. The values of BS/BV (Figure 3C), Tb.Sp (Figure 3G), SMI (Figure 3H), and Tb.Pf (Figure 3I) increased while the values of BV/TV (Figure 3D) and Tb.Th (Figure 3F) decreased in the model group, showing structural changes in the trabecular bone after VCD exposure. BSNXD

treatment significantly reverses these parameters' change, improving the bone microstructure of the murine femur. There were no indistinguishable changes in the cancellous BMD (Tb.BMD, Figure 3J) and cortical BMD (Ct.BMD, Figure 3K) among the three groups, probably due to the short period of the experiment.

### 3.4. BSNXD inhibited the differentiation and maturity of the osteoclast

Bone remodeling depends on the balance of the number and function of osteoblasts and osteoclasts (23). To determine the impact of BSNXD on osteoblasts or osteoclasts, we quantitatively analyzed bone turnover parameters and histological morphology *via* toluidine blue and TRAP staining. The bone histomorphometric parameters indicated an increased number of osteoblasts and osteoclasts after VCD treatment (Figures 4A–4C). BSNXD could reduce the osteoclast number (Figures 4A, 4C) but have no obvious inhibitory effect on the osteoblast number (Figures 4A–4B). Next, to investigate whether BSNXD inhibits osteoclast differentiation, we induced each group's murine bone marrow-derived macrophages to differentiate *in vitro*. The number of TRAP<sup>+</sup> cells increased in the model group on day 7 according to the number of nuclei (Figure 4D). Meanwhile, BSNXD treatment decreased the number of TRAP<sup>+</sup> multinucleated cells (Figure 4D). We also detected the gene expression related to osteoclastogenesis and osteoclasts' function. BSNXD treatment led to significantly reduced gene expression of *Trap*, matrix metalloprotein 9 (*Mmp9*), cathepsin K (*Ctsk*), *c-fos*, *Nfatc1*, and *Rankl* compared with the model group (Figure 4E), presenting a significant impact of BSNXD on osteoclastogenesis and osteoclast maturity.

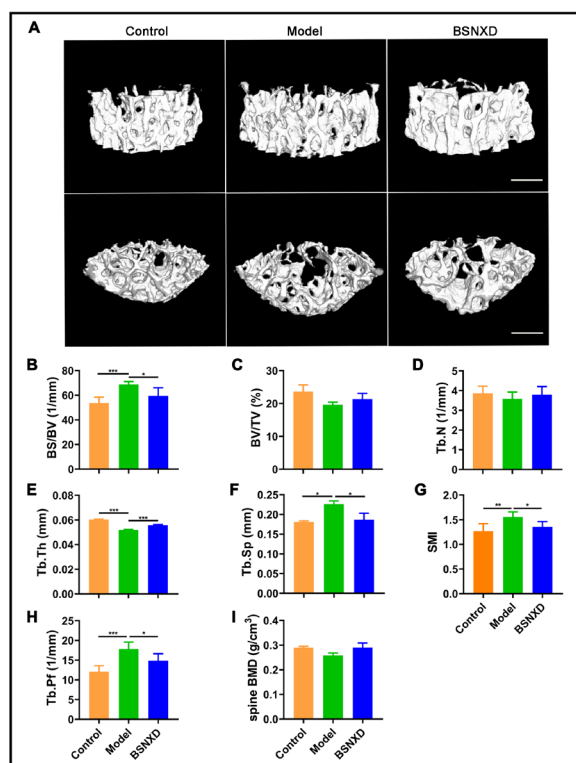


**Figure 2.** BSNXD treatment protected against bone loss in the lumbar vertebra in the VCD-induced POI model. (A) Representative 3D images of the 4th lumbar vertebra. Scale bars are 0.1 mm. (B-I) Comparative analysis of the bone structural parameters: (B) BS/BV, (C) BV/TV, (D) Tb.N, (E) Tb.Th, (F) Tb.Sp, (G) SMI, (H) Tb.Pf, and (I) spine BMD.  $n = 5$ . \* $P < 0.05$ , \*\* $P < 0.01$ , \*\*\* $P < 0.001$ .

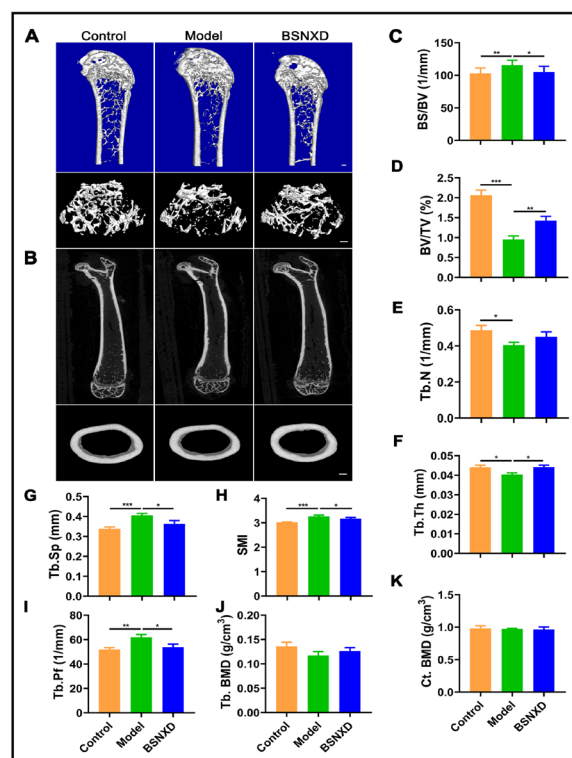


**Figure 3.** BSNXD treatment ameliorated the bone microstructure parameters in the femoral bone in the VCD-induced POI model. (A-B) Representative 3D reconstruction images of (A) cancellous and (B) cortical bone in the femur. Scale bars are 0.25 mm. (C-K) Comparative analysis of the trabecular parameters of the femur: (C) BS/BV, (D) BV/TV, (E) Tb.N, (F) Tb.Th, (G) Tb.Sp, (H) SMI, (I) Tb.Pf, (J) Tb.BMD, and (K) Ct.BMD.  $n = 5$ . \* $P < 0.05$ , \*\* $P < 0.01$ , \*\*\* $P < 0.001$ .

### 3.5. Network pharmacology predicted potential mechanisms of BSNXD regulating the POI-related osteoimmune disorder

#### 3.5.1. The intersection targets between BSNXD and POI-related osteoimmune disorder

To elaborate on the underlying therapeutic mechanism, we applied network pharmacology to determine the potential candidate compounds of BSNXD, which consists of the dried root of *Rehmannia glutinosa* (Gaertn.) DC., rhizomes of *Anemarrhena asphodeloides* Bunge, *Phellodendron chinense* C.K.Schneid., seed of *Lycium chinense* Mill., *Cuscuta chinensis* Lam., *Epimedium brevicornu* Maxim., seed of *Ziziphus jujuba var. spinosa* (Bunge) Hu ex H.F.Chow., and *Alisma plantago-aquatica* L. (Table 1). One hundred and fifty-three candidate compounds of BSNXD were obtained based on the oral bioavailability and drug likeness (Table S1, <http://www.ddtjournal.com/action/getSupplementalData.php?ID=197>), some of which, including quercetin, kaempferol, beta-sitosterol, and anhydroicaritin, have been identified in the BSNXD fingerprint analysis (14). Figure 5A shows the components-targets network of BSNXD. Two hundred forty-three compound targets were sorted

out using the TCMSP and HERB databases (Figure 5B). A total of 1264 POI and osteoimmune disorder-related targets were obtained using the OMIM, GeneCards, and Digenst databases. The Venn analysis diagrams shows the intersection targets of BSNXD against POI-related osteoimmune disorder, illustrating 127 overlapping targets (Figure 5B).

#### 3.5.2. PPI network construct

Next, we utilized the 127 proteins to construct a preliminary network in the STRING database and obtained the PPI network, which was re-edited by Cytoscape software (Figure 5C). The node degree average is 45. The top 20 hub targets were screened out (Figure 5D), representing a greater probability that the active ingredients will act on these targets.

#### 3.5.3. GO and KEGG analysis

To assess the involved signaling pathway regulated by BSNXD, we performed GO and KEGG enrichment analysis for the top 20 hub targets using the Metascape database. As shown in Figure 5E, the core genes were enriched to 687 biological process entries, 16 cellular

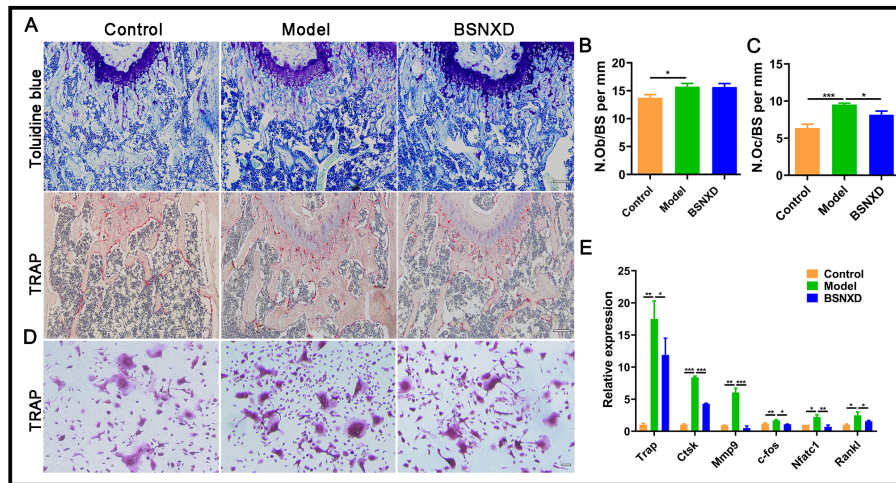


**Figure 4.** BSNXD treatment inhibited osteoclastogenesis in the VCD-induced POI model. (A) Histological analysis of the tibia bones, including toluidine blue and TRAP staining. (B-C) Quantitative analysis of (A): (B) N.Ob/BS and (C) N.Oc/BS. Scale bar represents 100  $\mu$ m (toluidine blue and TRAP staining). Murine bone marrow-derived macrophages from each group were cultured for RNAKL-induced osteoclastogenesis. (D) Representative images of TRAP staining after seven days of osteoclast differentiation. Scale bars present 50  $\mu$ m. (E) The gene expression of *Trap*, *Ctsk*, *Mmp9*, *c-fos*, *Nfatc1*, and *Rankl* in murine tibial bone.  $n = 3$ . \* $P < 0.05$ , \*\* $P < 0.01$ , \*\*\* $P < 0.001$ .

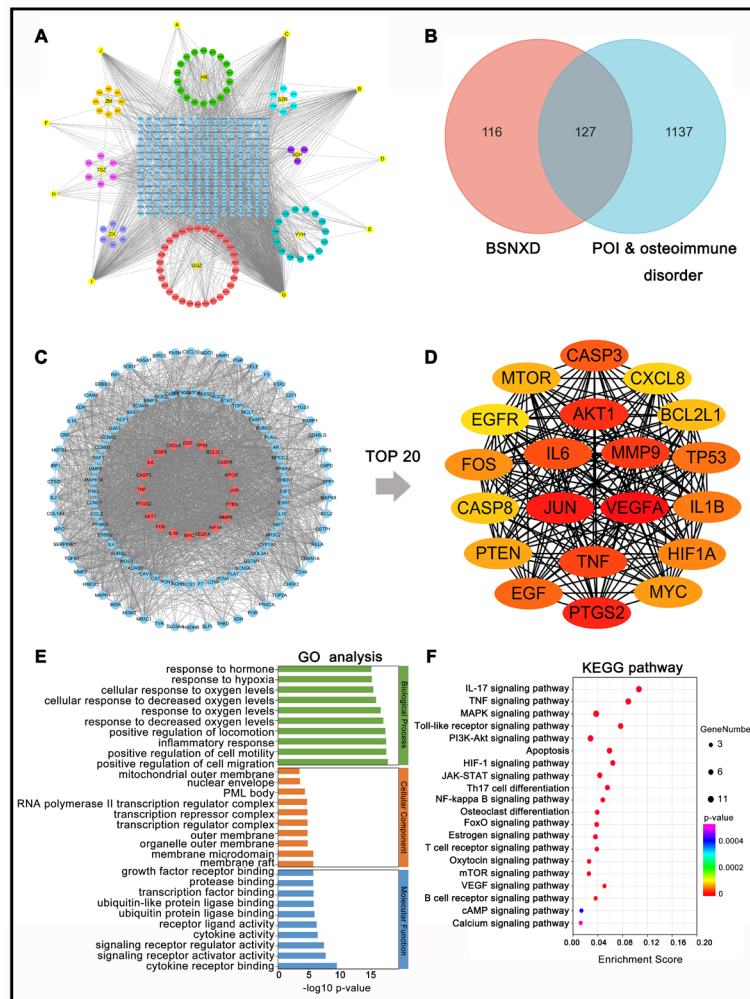


**Figure 5.** Network pharmacology predicted the action mechanisms of BSNXD on POI-related osteoimmune disorder. (A) Components-targets network. The blue diamond in the middle represents the compound target; the eight circles in different colors are different kinds of herbs and their active compounds in BSNXD; the outermost yellow circles are the common targets of the eight herbs. (B) The regulatory genes of BSNXD against POI-related osteoimmune disorder. (C) PPI network of the core regulatory targets. Red circles represent the top 20 targets, and blue circles represent other targets after the re-edition. (D) PPI network of the top 20 targets. The oval defines targets, and the one with the darker color defines a greater degree of centrality. (E) The GO pathway enrichment analysis: Green columns represent biological process; orange columns represent cellular composition; blue columns represent molecular function. (F) The KEGG pathway enrichment analysis.

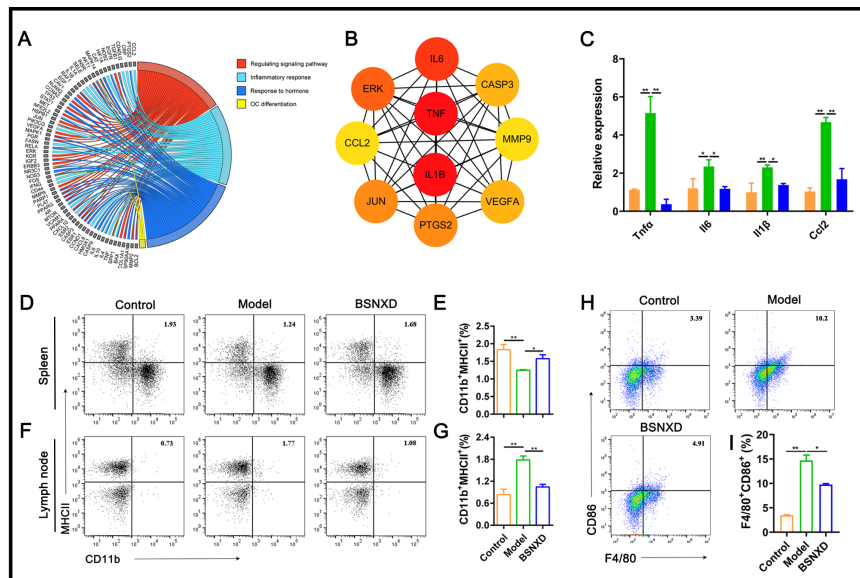


**Figure 6. BSNXD treatment regulated osteoimmune disorder via inhibiting macrophage activation.** (A) GO chord analysis obtained the intersection targets among response to inflammation, response to hormone, and osteoclast differentiation. (B) Hub targets were identified from (A). (C) The gene expression of *Tnfa*, *Il6*, *Il1b*, and *Ccl2* in murine tibial bone. (D-G) Flow cytometric analysis: CD11b<sup>+</sup>MHCII<sup>+</sup> cell percentage in (D-E) spleen and (F-G) mesenteric lymph nodes; (H-I) CD3<sup>+</sup>CD11b<sup>+</sup>F4/80<sup>+</sup>CD86<sup>+</sup> cell percentage in bone marrow. *n* = 3. \**P* < 0.05, \*\**P* < 0.01.

composition entries, and 36 molecular function entries. The top 20 biological processes involve signaling receptor regulator activity, signaling receptor activator activity, receptor ligand activity, cytokine activity, and positive regulation of cell migration. One hundred sixteen signaling pathways related to BSNXD against POI-related osteoimmune disorder were enriched. The top 20 pathways include the TNF signaling pathway, MAPK signaling pathway, osteoclast differentiation, and other signaling pathways (Figure 5F), suggesting the underlying mechanisms of BSNXD were closely associated with inflammation response and osteoclast differentiation.

### 3.6. BSNXD regulated macrophage activation in the VCD-induced POI mice

VCD exposure leads to increased FSH levels, playing a vital role in bone loss during menopause (9,24). Considering FSH evokes an inflammation response (10,11), we hypothesized that BSNXD may lead to inflammation regression to balance osteoclast differentiation and function. Thus, we performed bioinformatics analysis to assess the intersection targets among response to inflammation, response to hormone, and osteoclast differentiation (Figure 6A). Ten hub genes were screened using the Cytoscape software (Figure 6B); in particular, BSNXD treatment downregulated inflammatory factors, including *Tnfa*, interleukin (*Il*)6, *Il1b*, and chemokine (CC-motif) ligand (*Ccl*) 2 (Figure 6C). CCL2, known as monocyte chemotactic protein 1, leads to the migration and infiltration of inflammatory cells like monocytes/macrophages to the site of inflammation (25). Thus, we explored

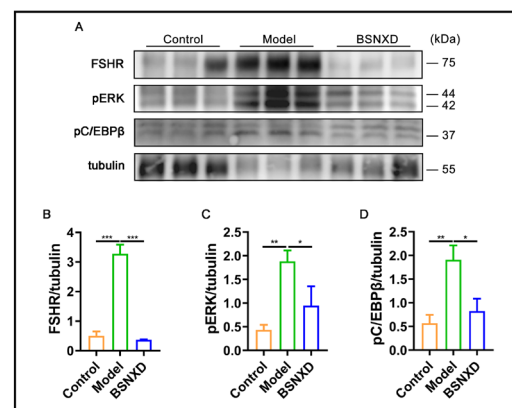


**Figure 7. BSNXD treatment inhibited the FSH/FSHR pathway.** (A) Western blotting of proteins from the murine bone tissue. (B-D) Quantifications of the protein expressions: (B) FSHR, (C) pC/EBPβ, and (D) pERK. *n* = 3. \**P* < 0.05, \*\**P* < 0.01, \*\*\**P* < 0.001.

the proportions of macrophages and monocytes, a primary source of *Tnfa*, *Il6*, and *Il1b*. Interestingly, we found a significant expansion of activated monocytes (CD11b<sup>+</sup>MHCII<sup>+</sup>) in the mesenteric lymph nodes and macrophages (CD3<sup>+</sup>CD11b<sup>+</sup>F4/80<sup>+</sup>CD86<sup>+</sup>) in the bone marrow but a reduction of activated monocytes in the spleen in the model mice. BSNXD reversed the changes, demonstrating its role in cell migration. These findings indicated that inflammation regulation of BSNXD was responsible for the POI-related osteoimmune disorder.

### 3.7. BSNXD inhibited macrophage activation by antagonizing the FSH/FSHR pathway

FSH binds to FSHR to activate macrophages by regulating downstream pathways and transcription

factor C/EBP $\beta$  (11). Western blotting indicates elevated FSHR, pERK, and pC/EBP $\beta$  levels after VCD exposure (Figure 7), mainly due to the increased FSH levels. Notably, BSNXD decreased the FSHR expression and inhibited the phosphorylated level of ERK and C/EBP $\beta$  (Figures 7A, 7C-7D), indicating BSNXD suppressed the macrophage activation *via* regulating the FSH/FSHR pathway.

#### 4. Discussion

Premenopause before the age of 40 years is linked to premature osteoporosis and fracture risk (26,27), attracting more attention to women with POI-related osteoporosis. In this work, BSNXD restrained osteoclast differentiation to ameliorate osteoimmune disorder in the VCD-induced murine POI model. Then, network pharmacology predicted the potential mechanisms of BSNXD against POI-related osteoimmune disorder involving TNF $\alpha$  and MAPK signaling pathways. The potential targets involving response to inflammation, response to hormone, and osteoclast differentiation were further validated by molecular biology experiments. Our results demonstrated that BSNXD inhibited the macrophage activation to reduce osteoclastogenesis by inhibiting the FSH/FSHR pathway.

VCD can selectively destroy the primordial and primary follicles to deplete the follicle reserve pool, leading to ovarian dysfunction (28,29). We successfully replicated a POI-related osteoimmune disorder murine model, distinguished by elevated serum FSH level, increased follicle destruction, macrophage activation, and impaired bone microstructure in the vertebrae and femur after VCD exposure. Despite follicle depletion in the POI mice, the ovaries appear to produce estradiol, leading to obviously increased E2 levels. It is consistent with the previous study that serum E2 levels were raised or remained unchanged in the early stage in the VCD-induced mice (30,31), mainly owing to remaining functional granulosa cells secreting E2 (32). Compared to ovariectomy, VCD modeling preserves part of the ovarian tissue and indicates a slow change of hormone levels, visually imitating human POI. Although we did not observe remarked changes in the trabecular and cortical BMD 30 days after the final VCD injection, there were impaired bone microstructures, including increased Tb.Sp and decreased BV/TV, Tb.Th, and Tb.N in the murine vertebrae or femur, inconsistent with the literature reports (18). It may be because a 45-day period in the VCD-induced POI mice is still in its early stages, only showing an osteoimmune disorder accompanied by a high bone turnover. Accelerated bone remodeling is usually characterized by an augmented number of osteoblasts and osteoclasts (23). Inspiringly, BSNXD treatment ameliorated the impaired bone microstructures, mainly due to the reduced number of osteoclasts but not osteoblasts. Considering c-fos/NFATc1 signaling is

a confirmed target to inhibit osteoclast differentiation (33,34), we identified that BSNXD treatment inhibited osteoclastogenesis *via* suppressing the osteoclastic mRNA expression (*Nfatc1*, *Ctsk*, *Trap*, *Mmp9*), consistent with our previous work (15).

Network pharmacology is an effective tool to reveal the pharmacology mechanism of the TCM formula (35). Based on this, we utilized network pharmacology to evaluate the potential mechanisms of BSNXD against the POI-related osteoimmune disorder. We filtered 153 bioactive compounds and predicted the top 20 core targets, including TNF, IL6, and IL1 $\beta$ , which may play central roles in BSNXD treating the POI-related osteoimmune disorder. The GO and KEGG analysis indicated that the mechanisms of BSNXD in relieving the POI-related osteoimmune disorder were possibly associated with the TNF and MAPK signaling pathways. Previous studies have confirmed that some BSNXD-related bioactive components inhibited osteoclastogenesis. For example, alisol C 23-acetate treatment lowered serum levels of TNF $\alpha$ , IL6, and IL1 $\beta$  and inhibited RANKL-induced osteoclast differentiation and function against osteoporosis (36). The top two active ingredients derived from BSNXD are quercetin and kaempferol, which are efficacious in suppressing osteoclastogenesis and bone resorption (37). Further studies confirmed these anti-inflammatory properties could inhibit osteoclastogenesis (38,39). These studies suggest that BSNXD might inhibit osteoclast differentiation by regulating inflammation.

Emerging evidence shows that menopausal transition prompts chronic low-grade inflammation due to FSH or estrogen changes (9,40,41). VCD can increase serum FSH levels, which causes hypogonadal bone loss independent of estrogen (10). FSH stimulates macrophages to produce TNF, which enhances osteoclast over-formation and causes bone remodeling disorder (9). Our results showed an increased ratio of activated monocytes from the mesenteric lymph nodes and bone marrow but a reduced ratio of activated monocytes from the spleen, accompanied by a high expression of CCL2, probably resulting in activated monocyte migration. Next, we utilized bioinformatics analysis to minify the potential targets of BSNXD ameliorating POI-related osteoimmune disorder. Of note, ten molecules, including TNF, IL1 $\beta$ , IL6, MMP9, CCL2, ERK, JUN, CASP3, PTGS2, and VEGFA, were identified, among which TNF $\alpha$  and IL1 $\beta$  are bone-reabsorbing cytokines (42). BSNXD treatment suppressed the bone gene expression of TNF, IL1 $\beta$ , IL6, CCL2, and MMP9 and regulated the ratio of activated macrophages in the different tissues, showing vital impacts of BSNXD on the activation and migration of monocytes/macrophages. FSH binds to FSHR on the surface of monocytes/macrophages to induce MEK/Erk and C/EBP $\beta$  phosphorylation, stimulating TNF production to enhance osteoclast differentiation (10,11). As we speculated, BSNXD

downregulated the FSHR expression and inhibited the ERK and C/EBP $\beta$  phosphorylation in the POI-relative osteoimmune disorder, indicating BSNXD suppressed the macrophage activation *via* regulating the FSH/FSHR pathway.

In summary, BSNXD suppressed osteoclast differentiation by regulating the inflammatory response. More specifically, BSNXD inhibited the macrophage activation to reduce osteoclastogenesis by downregulating the FSHR expression and inhibiting the ERK and C/EBP $\beta$  phosphorylation. However, considering that VCD can induce osteoporosis after 75 days or more treatment, the effects of BSNXD on the disease's different stages need to be studied. Moreover, the direct or indirect action of how BSNXD regulates macrophage activation to inhibit osteoclast differentiation needs further elaboration.

**Funding:** This work was supported by grants from a project of the National Natural Science Foundation of China (grant No. 82374243 to L Wang) and a project of the Natural Science Foundation of Gansu province (grant No. 23JRRG0009 to HM Sun).

**Conflict of Interest:** The authors have no conflicts of interest to disclose.

## References

- Golezar S, Ramezani Tehrani F, Khazaei S, Ebadi A, Keshavarz Z. The global prevalence of primary ovarian insufficiency and early menopause: A meta-analysis. *Climacteric*. 2019; 22:403-411.
- Stuenkel CA, Gompel A. Primary ovarian insufficiency. *N Engl J Med*. 2023; 388:154-163.
- Qin X, Zhao Y, Zhang T, Yin C, Qiao J, Guo W, Lu B. TrkB agonist antibody ameliorates fertility deficits in aged and cyclophosphamide-induced premature ovarian failure model mice. *Nat Commun*. 2022; 13:914.
- Ding L, Yan G, Wang B, *et al*. Transplantation of UC-MSCs on collagen scaffold activates follicles in dormant ovaries of POF patients with long history of infertility. *Sci China Life Sci*. 2018; 61:1554-1565.
- Zhang X, Lu Y, Wu S, Zhao X, Li S, Zhang S, Tan J. Estimates of global research productivity in primary ovarian insufficiency from 2000 to 2021: Bibliometric analysis. *Front Endocrinol (Lausanne)*. 2022; 13:959905.
- Uehara M, Wada-Hiraike O, Hirano M, Koga K, Yoshimura N, Tanaka S, Osuga Y. Relationship between bone mineral density and ovarian function and thyroid function in perimenopausal women with endometriosis: A prospective study. *BMC Womens Health*. 2022; 22:134.
- Wu XY, Wu XP, Xie H, Zhang H, Peng YQ, Yuan LQ, Su X, Luo XH, Liao EY. Age-related changes in biochemical markers of bone turnover and gonadotropin levels and their relationship among Chinese adult women. *Osteoporos Int*. 2010; 21:275-285.
- Chin KY. The Relationship between follicle-stimulating hormone and bone health: Alternative explanation for bone loss beyond oestrogen? *Int J Med Sci*. 2018; 15:1373-1383.
- Zhu D, Li X, Macrae VE, Simoncini T, Fu X. Extragonadal effects of follicle-stimulating hormone on osteoporosis and cardiovascular disease in women during menopausal transition. *Trends Endocrinol Metab*. 2018; 29:571-580.
- Sun L, Peng Y, Sharrow AC, *et al*. FSH directly regulates bone mass. *Cell*. 2006; 125:247-260.
- Xiong J, Kang SS, Wang Z, *et al*. FSH blockade improves cognition in mice with Alzheimer's disease. *Nature*. 2022; 603:470-476.
- Liu X, Song Y, Zhou F, Zhang C, Li F, Hu R, Ma W, Song K, Tang Z, Zhang M. Network and experimental pharmacology on mechanism of Si-Wu-tang improving ovarian function in a mouse model of premature ovarian failure induced by cyclophosphamide. *J Ethnopharmacol*. 2023; 301:115842.
- Peng Z, Xu R, You Q. Role of traditional Chinese medicine in bone regeneration and osteoporosis. *Front Bioeng Biotechnol*. 2022; 10:911326.
- Wang L, Qiu XM, Gui YY, Xu YP, Gober HJ, Li DJ. Bu-Shen-Ning-Xin decoction ameliorated the osteoporotic phenotype of ovariectomized mice without affecting the serum estrogen concentration or uterus. *Drug Des Devel Ther*. 2015; 9:5019-5031.
- Wang L, Qiu XM, Gui YY, Xu YP, Gober HJ, Li DJ. Bu-Shen-Ning-Xin decoction: Inhibition of osteoclastogenesis by abrogation of the RANKL-induced NFATc1 and NF- $\kappa$ B signaling pathways *via* selective estrogen receptor  $\alpha$ . *Drug Des Devel Ther*. 2015; 9:3755-3766.
- Gui Y, Qiu X, Xu Y, Li D, Wang L. Bu-Shen-Ning-Xin decoction suppresses osteoclastogenesis *via* increasing dehydroepiandrosterone to prevent postmenopausal osteoporosis. *Biosci Trends*. 2015; 9:169-181.
- Zhang JL, Qiu XM, Zhang N, Tang W, Gober HJ, Li DJ, Wang L. Bu-Shen-Ning-Xin decoction suppresses osteoclastogenesis by modulating RANKL/OPG imbalance in the CD4<sup>+</sup> T lymphocytes of ovariectomized mice. *Int J Mol Med*. 2018; 42:299-308.
- Cao LB, Leung CK, Law PW, Lv Y, Ng CH, Liu HB, Lu G, Ma JL, Chan WY. Systemic changes in a mouse model of VCD-induced premature ovarian failure. *Life Sci*. 2020; 262:118543.
- Lukefahr AL, Frye JB, Wright LE, Marion SL, Hoyer PB, Funk JL. Decreased bone mineral density in rats rendered follicle-deplete by an ovotoxic chemical correlates with changes in follicle-stimulating hormone and inhibin A. *Calcif Tissue Int*. 2012; 90:239-249.
- Nogales C, Mamdouh ZM, List M, Kiel C, Casas AI, Schmidt H. Network pharmacology: Curing causal mechanisms instead of treating symptoms. *Trends Pharmacol Sci*. 2022; 43:136-150.
- Vanden Brink H, Pisch AJ, Lujan ME. A comparison of two- and three-dimensional ultrasonographic methods for evaluation of ovarian follicle counts and classification of polycystic ovarian morphology. *Fertil Steril*. 2021; 115:761-770.
- Qi Q, Chen L, Sun H, Zhang N, Zhou J, Zhang Y, Zhang X, Li L, Li D, Wang L. Low-density lipoprotein receptor deficiency reduced bone mass in mice *via* the c-fos/NFATc1 pathway. *Life Sci*. 2022; 310:121073.
- Wang L, You X, Zhang L, Zhang C, Zou W. Mechanical regulation of bone remodeling. *Bone Res*. 2022; 10:16.
- Fischer V, Haffner-Luntzer M. Interaction between bone and immune cells: Implications for postmenopausal osteoporosis. *Semin Cell Dev Biol*. 2022; 123:14-21.

25. Singh S, Anshita D, Ravichandiran V. MCP-1: Function, regulation, and involvement in disease. *Int Immunopharmacol.* 2021; 101:107598.
26. Sullivan SD, Lehman A, Thomas F, Johnson KC, Jackson R, Wactawski-Wende J, Ko M, Chen Z, Curb JD, Howard BV. Effects of self-reported age at nonsurgical menopause on time to first fracture and bone mineral density in the Women's health initiative observational study. *Menopause.* 2015; 22:1035-1044.
27. Sullivan SD, Lehman A, Nathan NK, Thomson CA, Howard BV. Age of menopause and fracture risk in postmenopausal women randomized to calcium + vitamin D, hormone therapy, or the combination: Results from the Women's health initiative clinical trials. *Menopause.* 2017; 24:371-378.
28. Song W, Li A, Sha QQ, Liu SY, Zhou Y, Zhou CY, Zhang X, Li XZ, Jiang JX, Li F, Li C, Schatten H, Ou XH, Sun QY. Maternal exposure to 4-vinylcyclohexene diepoxide during pregnancy induces subfertility and birth defects of offspring in mice. *Sci Total Environ.* 2023; 859:160431.
29. Konhilas JP, Sanchez JN, Regan JA, Constantopoulos E, Lopez-Pier M, Cannon DK, Skaria R, McKee LA, Chen H, Lipovka Y, Pollow D, Brooks HL. Using 4-vinylcyclohexene diepoxide as a model of menopause for cardiovascular disease. *Am J Physiol Heart Circ Physiol.* 2020; 318:H1461-h1473.
30. Lohff JC, Christian PJ, Marion SL, Arrandale A, Hoyer PB. Characterization of cyclicity and hormonal profile with impending ovarian failure in a novel chemical-induced mouse model of perimenopause. *Comp Med.* 2005; 55:523-527.
31. Brooks HL, Pollow DP, Hoyer PB. The VCD mouse model of menopause and perimenopause for the study of sex differences in cardiovascular disease and the metabolic syndrome. *Physiology (Bethesda).* 2016; 31:250-257.
32. Carolino ROG, Barros PT, Kalil B, Anselmo-Franci J. Endocrine profile of the VCD-induced perimenopausal model rat. *PLoS One.* 2019; 14:e0226874.
33. Ma JD, Jing J, Wang JW, Mo YQ, Li QH, Lin JZ, Chen LF, Shao L, Miossec P, Dai L. Activation of the peroxisome proliferator-activated receptor  $\gamma$  coactivator 1 $\beta$ /NFATc1 pathway in circulating osteoclast precursors associated with bone destruction in rheumatoid arthritis. *Arthritis Rheumatol.* 2019; 71:1252-1264.
34. Zhang L, Yang Y, Liao Z, Liu Q, Lei X, Li M, Saijilafu, Zhang Z, Hong D, Zhu M, Li B, Yang H, Chen J. Genetic and pharmacological activation of hedgehog signaling inhibits osteoclastogenesis and attenuates titanium particle-induced osteolysis partly through suppressing the JNK/c-Fos-NFATc1 cascade. *Theranostics.* 2020; 10:6638-6660.
35. Zhao L, Zhang H, Li N, Chen J, Xu H, Wang Y, Liang Q. Network pharmacology, a promising approach to reveal the pharmacology mechanism of Chinese medicine formula. *J Ethnopharmacol.* 2023; 309:116306.
36. Jia X, Zhu H, Li G, Lan M, Li X, Huang M, Xu W, Wu S. Anti-osteoporotic effects of alisol C 23-acetate *via* osteoclastogenesis inhibition. *Biomed Pharmacother.* 2021; 137:111321.
37. An J, Hao D, Zhang Q, Chen B, Zhang R, Wang Y, Yang H. Natural products for treatment of bone erosive diseases: The effects and mechanisms on inhibiting osteoclastogenesis and bone resorption. *Int Immunopharmacol.* 2016; 36:118-131.
38. Pandey MK, Gupta SC, Karelia D, Gilhooley PJ, Shakibaei M, Aggarwal BB. Dietary nutraceuticals as backbone for bone health. *Biotechnol Adv.* 2018; 36:1633-1648.
39. Wong SK, Chin KY, Ima-Nirwana S. The osteoprotective effects of kaempferol: The evidence from *in vivo* and *in vitro* studies. *Drug Des Devel Ther.* 2019; 13:3497-3514.
40. McCarthy M, Raval AP. The peri-menopause in a woman's life: A systemic inflammatory phase that enables later neurodegenerative disease. *J Neuroinflammation.* 2020; 17:317.
41. Yasui T, Maegawa M, Tomita J, Miyatani Y, Yamada M, Uemura H, Matsuzaki T, Kuwahara A, Kamada M, Tsuchiya N, Yuzurihara M, Takeda S, Irahara M. Changes in serum cytokine concentrations during the menopausal transition. *Maturitas.* 2007; 56:396-403.
42. Charatcharoenwitthaya N, Khosla S, Atkinson EJ, McCready LK, Riggs BL. Effect of blockade of TNF- $\alpha$  and interleukin-1 action on bone resorption in early postmenopausal women. *J Bone Miner Res.* 2007; 22:724-729.

Received January 29, 2024; Revised April 8, 2024; Accepted April 11, 2024.

§These authors contributed equally to this work.

\*Address correspondence to:

Ling Wang, Laboratory for Reproductive Immunology, Obstetrics and Gynecology Hospital of Fudan University, 419 Fangxie Road, Shanghai 200011, China.  
E-mail: Dr.wangling@fudan.edu.cn

Released online in J-STAGE as advance publication pril 17, 2024.